Ab Initio Study on the Oxidation of NCN by O (^{3}P): Prediction of the Total Rate Constant and Product Branching Ratios†

R. S. Zhu* and M. C. Lin

Department of Chemistry, Emory University, Atlanta, Georgia 30322

Received: December 28, 2006; In Final Form: March 17, 2007

The reaction of NCN with O is relevant to the formation of prompt NO according to the new mechanism, CH + N_2 → cyclic-C(H)NN− → HNCN → H + NCN. The reaction has been investigated by ab initio molecular orbital and transition state theory calculations. The mechanisms for formation of possible product channels involved in the singlet and triplet potential energy surfaces have been predicted at the highest level of the modified GAUSSIAN-2 (G2M) method, G2M (CC1). The barrierless association/dissociation processes on the singlet surface were also examined with the third-order Rayleigh−Schrödinger perturbation (CASPT3) and the multireference configuration interaction methods including Davidson's correction for higher excitations (MRCI+Q) at the CASPT3(6,6)/6-311+G(3df)//UB3LYP/6-311G(d) and MRCI+Q(6,6)/6-311+G(3df)//UB3LYP/6-311G(d) levels. The rate constants for the low-energy channels producing CO + N_2, CN + NO, and N(^{4}S) + NCO have been calculated in the temperature range of 200−3000 K. The results show that the formation of CN + NO is dominant and its branching ratio is over 99% in the whole temperature range; no pressure dependence was noted at pressures below 100 atm. The total rate constant can be expressed by: $k_t = 4.23 \times 10^{-11}\, T^{0.15} \exp(17/T)$ cm^3 molecule^{-1} s^{-1}.

I. Introduction

The reaction of CH with molecular nitrogen has been predicted to be responsible for the "prompt NO" formation. Fenimore[1] first proposed the mechanism in 1971, CH + N_2 → N + HCN, where the products N and HCN could then be rapidly oxidized into NO under combustion conditions. In 1977, Blauwens et al.[2] provided the first direct experimental evidence for the "prompt NO" formation by CH + N_2, based on Fenimore's mechanism (which is spin forbidden). In 2000, Lin and co-workers[3,4] put forth a new mechanism for the reaction of CH with N_2, based on high-level potential energy surface (PES) calculations. The reaction produces HNCN and/or H + NCN via a spin-allowed pathway, CH + N_2 → cyclic-C(H)-NN− → HNCN → H + NCN, the predicted rate constant is considerably more favorable than the long accepted Fenimore mechanism for prompt NO formation[1] in the primary zone of a hydrocarbon flame.[3,4] According to the new mechanism, the formation of NO can in principle result from the rapid oxidation of NCN and, to some extent, HNCN, by O, OH, and O_2 present in the primary flame zone.[3,4] As the kinetics of NCN radical reactions are not available in the literature, we have since computationally predicted the rate constants for some key reactions involving NCN for combustion modeling applications. In our previous work, we have reported the oxidation of NCN by O_2 at the G2M (CC1) level,[5] the results show that oxidation NCN by O_2 to produce NCO + NO and CNO + NO is very slow because of the high entrance and exit barriers.

In this work, the much faster and more exothermic oxidation reaction, NCN + ^{3}O, has been investigated. We have attempted to map out a detailed PES for the system and study the temperature and pressure effects on its rate constants for the reaction taking place along the low-lying energy pathways. The results of this study are presented herein. The following main association/decomposition pathways via singlet and triplet intermediates, NCNO (^{1}A′) and NCNO (^{3}A″), will be discussed

$$\mathrm{NCN + O\ (^3P) \rightarrow {}^1NCNO\ (^1A') \rightarrow CO + N_2} \quad (1)$$

$$\rightarrow \mathrm{CN + NO} \quad (2)$$

$$\mathrm{NCN + O\ (^3P) \rightarrow {}^3NCNO\ (^3A'') \rightarrow CN + NO} \quad (3)$$

$$\rightarrow \mathrm{N\ (^4S) + NCO} \quad (4)$$

The individual and total rate constants and product branching ratios are predicted in this work.

II. Computational Methods

The geometries of the reactants, intermediates, transition states, and products for the NCN + O(^{3}P) reaction were optimized at the hybrid density functional UB3LYP/6-311+G (3df) level of theory, i.e., Beck's three-parameter nonlocal-exchange functional[6−8] with the nonlocal correlation functional of Lee, Yang, and Parr.[9] The vibrational frequencies, calculated at this level were used for characterization of stationary points' zero-point energy (ZPE) corrections. All the stationary points were identified for local minima (with the number of imaginary frequencies equal to zero) and transition states (each with one imaginary frequency). Intrinsic reaction coordinate (IRC) calculations[10] were performed to confirm the connection between a transition state and designated intermediate. To obtain reliable energies, the PES was calculated using the highest scheme of the modified GAUSSIAN-2 (G2M) method, G2M (CC1),[11] which employed a series of calculations with the B3LYP optimized geometry to approximate the CCSD(T)/6-311+G-

† Part of the special issue "M. C. Lin Festschrift".

* To whom correspondence should be addressed. E-mail address: rzhu@emory.edu.

10.1021/jp068991b CCC: $37.00
Published on Web 04/26/2007

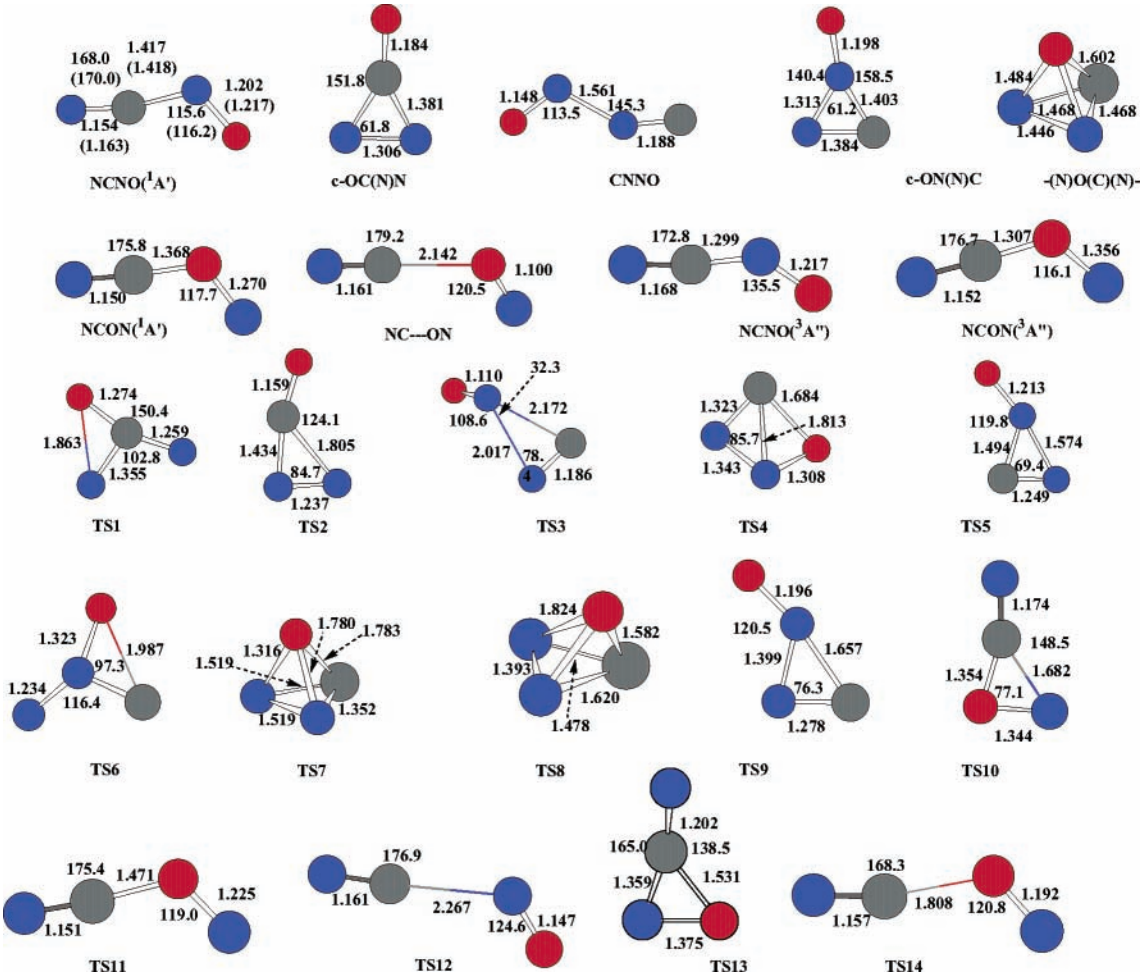

Figure 1. The optimized geometries of the intermediates, transition states at the B3LYP/6−311+G(3df) level. The values in the parenthesis for NCNO (^{1}A′) are the experimental data (ref 23). The bond lengths are given in angstroms and angles in degrees.

(3df,2p) level of theory, including a "higher level correction" based on the number of paired and unpaired electron.

The Gaussian 03 program[12] was used for the molecular orbital calculations. The rate constants were computed with the Variflex code.[13]

III. Results and Discussion

A. PES and Reaction Mechanism. The optimized geometries of the intermediates and transition states at the B3LYP/6-311+G(3df) level are shown in Figure 1. The singlet and triplet potential energy diagrams obtained at the G2M(CC1) level are presented in parts a and b of Figure 2, respectively, the vibrational frequencies and rotational constants of all species are summarized in Table 1.

CO + N_2 Formation. On the singlet surface, there are four possible pathways to form CO + N_2, which can be represented by the following Scheme 1:

The first pathway is that the interaction of O with NCN forms an open-chain NCNO (^{1}A′) molecule which is well-known both experimentally[14−24] and from theoretical studies.[25−30] As shown in Figure 1, calculated bond lengths and bond angles of NCNO (^{1}A′) are close to the experimental values,[23] the calculated frequencies are compared with the experimental data[23] in Table 1, the agreement is quite satisfactory. NCNO (^{1}A′) lies below the reactants by 93.5 kcal/mol at the G2M(CC1) level. The O atom in NCNO migrates to the C atom to form a more stable three-membered cyclic OC(N)N [denoted as c-OC(N)N] with C_{2v} symmetry via TS1. TS1 lies 13.3 kcal/mol below the reactants and 80.2 kcal/mol above the intermediate NCNO. c-OC(N)N is 15.4 kcal/mol more stable than NCNO, which can be compared with the values 13.8 and 15.9 kcal/mol, predicted by Korkin et al.[30] at the MP2/6-31 + G(d) and QCISD(T)/6-311 + G(d)//MP2/6-31+G(d) levels, respectively. As shown in Figure 1 and the above Scheme 1, c-OC(N)N can dissociate to CO + N_2 via TS2 in which the two breaking CN bonds lengthen 0.053 and 0.43 Å, respectively, compared with those in c-OC(N)N. The barrier height for N_2 elimination from c-OC(N)N is 25.6 kcal/mol.

The second pathway is that NCNO isomerizes to CNNO via TS3 with a looser structure, followed by dissociation to produce to CO + N_2 via a four-center transition state TS4. CNNO, TS3, and TS4 lie 20.0, 30.6, and 72.5 kcal/mol above NCNO, respectively.

The third pathway, as shown in Scheme 1, NCNO isomerizes to c-ON(N)C via TS5, then c-ON(N)C dissociates to CO + N_2 via TS6. The isomerization barrier height for the first step is 87.5 kcal/mol and the dissociation process for the last step needs a much high energy (28.5 kcal/mol above the reactants). Apparently, this channel is not competitive for the CO + N_2 formation.

On the last pathway, the C_{2v} c-OC(N)N isomerizes to form a tetrahedrane-like −(N)O(C)(N)− intermediate via TS7, followed by decomposition of −(N)O(C)(N)− to produce CO + N_2 via TS8 (see Figure 1). From the PES one can see that the −(N)O(C)(N)− molecule is unstable, it lies above the reactants by 2.5 kcal/mol. TS7 and TS8 lie above the reactants by 30.3

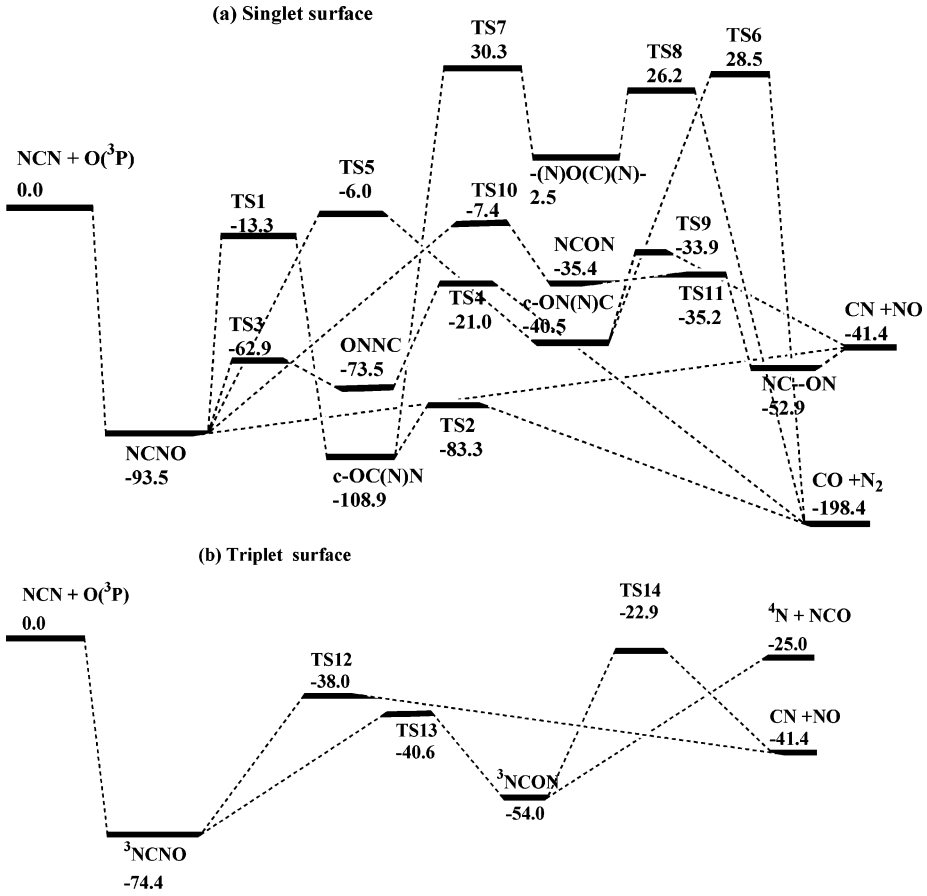

Figure 2. Energy diagrams (in kcal/mol) for the NCN−O system, computed at the G2M (CC1) level: (a) singlet surface; (b) triplet surface.

TABLE 1: Rotational Constant and Vibrational Frequencies of Reactants, Intermediates, and Transition States Computed at the B3LYP/6-311+G(3df) Level

species	I_a, I_b, I_c (GHZ)	frequencies (cm^{-1})
NCN	12.00, 12.00, 0.0	449.1, 449.1, 1274.3, 1566.7
NCNO ($^1A'$)	90.5, 5.4, 5.1	233.1, 288.8, 650.9, 723.1, 1570.7, 2263.1 (217), (264), (589), (820), (1501). (2170)[a]
c-OC(N)N	42.6, 8.5, 7.1	536.3, 582.9, 944.6, 969.9,1421.9, 2058.6
CNNO	104.2, 5.4, 5.2	84.0, 175.2, 318.7, 744.1, 1770.8, 2052.7
c-ON(N)C	41.3, 9.1, 7.5	458.7, 549.4, 864.7,1145.1,1317.5,1791.5
−(N)O(C)(N)−	18.0, 15.8, 15.3	550.5, 684.4, 848.7, 866.2, 955.5, 1289.6
NCON	75.6, 5.6, 5.2	221.5, 346.5, 550.2, 773.9, 1195.8, 2309.6
^{3}NCNO ($^3A''$)	168.7, 5.0, 4.9	224.0, 417.7, 572.1, 948.3, 1665.7, 2115.9
^{3}NCON ($^3A''$)	65.1, 5.8, 5.3	240.0, 471.9, 583.7, 943.3, 1120.0, 2352.4
TS1	21.8, 11.1, 7.5	565.4*i*, 389.5, 527.2, 866.7, 1228.9, 1707.9
TS2	41.7, 7.4, 6.3	909.4*i*, 397.6, 399.2, 813.2,1543.9, 2055.9
TS3	34.5, 6.0,5.7	321.6*i*, 169.2, 323.5, 532.4, 2013.3, 2081.5
TS4	23.8, 14.5, 9.4	528.3*i*, 589.5, 932.3, 1020.6, 1203.7, 1392.5
TS5	49.8, 7.7, 6.7	990.1*i*, 92.2, 356.2, 645.2, 1494.0, 1713.0
TS6	20.1, 11.7, 7.5	660.3*i*, 367.8, 558.3, 1024.5, 1344.2, 1470.3
TS7	22.2, 13.0,12.2	907.2*i*, 300.8, 507.1, 938.8, 1069.5,1271.4
TS8	20.0, 14.9,11.9	1070.3*i*, 397.4, 655.3, 809.9, 947.5, 1309.7
TS9	51.4, 7.9, 6.8	589.3*i*, 311.6, 687.9, 727.7, 1575.6, 1669.3
TS10	39.0, 7.8, 6.5	780.3*i*, 391.7, 450.4, 798.4, 1115.4, 2066.8
TS11	82.2, 5.3,4.9	503.4*i*, 151.6, 210.5, 750.2, 1294.9, 2270.4
TS12	99.3, 3.1, 3.0	143.5*i*, 53.6, 68.0, 200.6, 1926.2, 2166.0
TS13	35.1, 8.4, 6.8	510.7*i*, 402.8, 487.3, 885.8, 1153.8, 1796.9
TS14	94.2, 4.2, 4.0	571.0*i*, 82.6, 95.3, 395.8, 1404.5, 2198.9

[a] The values in the parenthesis for NCNO ($^1A'$) are the experimental data (ref 23).

and 26.2 kcal/mol, respectively. Kinetically, this pathway is not competitive, either.

NC + NO Formation. To help understand the reaction pathways for the formation of NC + NO, the singlet and triplet PES diagrams were simplified by Schemes 2 and 3 as follows. There are five pathways to produce NC + NO via the singlet and triplet surfaces.

On the singlet surface as shown in Scheme 2, NCNO first isomerizes to c-ON(N)C via TS5, besides the decomposition of c-ON(N)C to CO + N_2 as discussed in the above section, c-ON(N)C can decompose to CN + NO via TS9 with only 6.6 kcal/mol barrier height. Second, NCNO isomerizes to NCON via TS10 with 86.1 kcal/mol barrier height, NCON readily converts to NC···ON complex via TS11 with only 0.2 kcal/

SCHEME 1

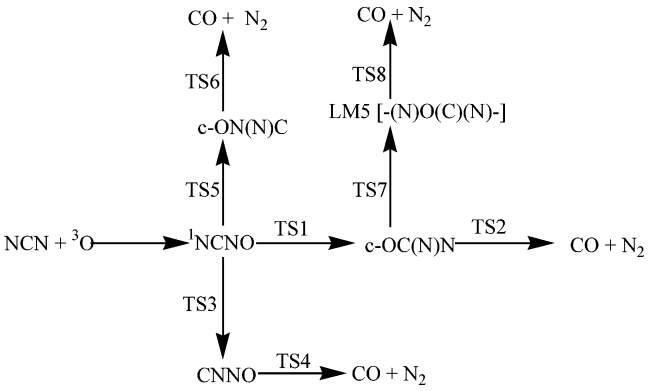

SCHEME 2

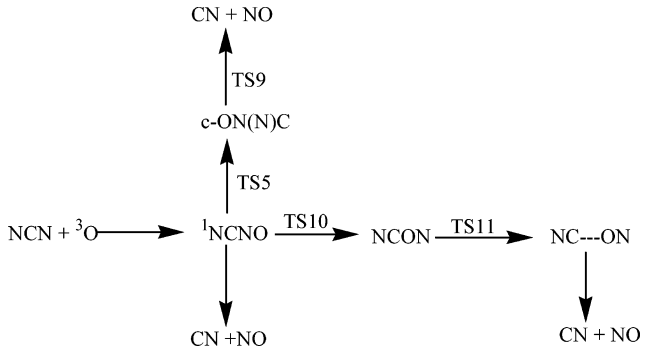

SCHEME 3

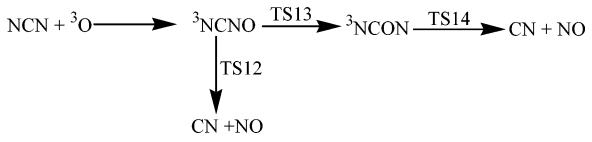

mol barrier. The NC···ON complex barrierlessly decomposes to CN + NO, which lies below the products CN + NO by 11.5 kcal/mol. Third, the singlet NCNO (^{1}A′) can barrierlessly dissociate to CN + NO lying below the reactants by 41.4 kcal/mol, this pathway can be expected as the dominant channel.

On the triplet surface as shown in Scheme 3, the interaction of the reactants can form triplet NCNO (^{3}A″) lying below the reactants by 74.4 kcal/mol, NCNO (^{3}A″) dissociates to CN + NO via TS12 with a 36.4 kcal/mol barrier. In addition, ^{3}NCNO isomerizes to ^{3}NCON via TS13, and ^{3}NCON decomposes to CN + NO via TS14. ^{3}NCON, TS13, and TS14 lie above NCNO (^{3}A″) by 20.4, 33.8, and 51.5 kcal/mol, respectively.

N (^{4}S) + NCO Formation. As shown in Figure 2b, the decomposition of ^{3}NCON can produce N (^{4}S) + NCO; this is a barrierless process.

B. Heats of Reaction for Different Channels. As shown in the PES diagrams (see parts a and b of Figure 2), the heats of reaction for the products CO + N_2, CN + NO and N (^{4}S) + NCO are −198.4, −41.4, and −25.0 kcal/mol, respectively. They are in good agreement with the experimental values, −197.5 ± 2.7, −43.3 ± 2.7, and −27.5 ± 1.14 kcal/mol based on the known experimental heats of formation (at 0 K) of NCN (111.3 ± 0.7 kcal/mol),[31] ^{3}O (59.0 ± 0.02 kcal/mol),[32] CO (−27.2 ± 0.04),[32] CN (105.5 ± 2 kcal/mol),[32] NO (21.46 ± 0.04 kca/mol),[32] ^{4}N(^{4}S) (112.5 ± 0.02 kcal/mol),[32] and NCO (30.3 ± 0.4 kcal/mol).[32] It should be mentioned that the JANAF recommended heat of formation has a large uncertainty (105.5 ± 2 kcal/mol)[32] for CN. The latest experimental value, determined using three methods by Halpern and co-workers,[33] is 104.1 ± 0.5 kcal/mol. More accurate values could be obtained by higher level calculation, such as using W4 theory established by Ruscic et al.,[34] which will not be discussed in this work.

TABLE 2: Dissociation Energies (in kcal/mol) for NCN−O and NC−NO at Different Levels

method	G2M(CC1)	CASPT3[a]	MRCI+Q[a]	exptl D_0[b]
NCN−O	93.5	99.0	94.6	N/A
NC−NO	52.1	54.4	51.6	48.85 ± 0.03

[a] The CASPT3 and MRCI+Q single-point energies are calculated at the CASPT3(6,6)/6-311+G(3df)//UB3LYP/6-311G(d) and MRCI+Q(6,6)/6-311+G(3df)//UB3LYP/6-311G(d), respectively. [b] Reference 21.

C. VTST Calculations for the Association/Decomposition Processes. Our test shows that the structure of NCNO obtained at the B3LYP/6-311+G(3df) level is close to that obtained at the B3LYP/6-311(d) level and the G2M(CC1) energies based on the structures obtained by the above basis sets have only 0.5 kcal/mol difference. Therefore, for the variational association/dissociation curves, they were calculated using the 6-311G(d) basis set. For the barrierless association process of NCN + ^{3}O → NCNO (^{1}A′) and the decomposition of NCNO (^{1}A′) → CN + NO, the potential energy curves were computed from the stable NCNO (^{1}A′) to cover the N−O and C−N bonds with separations from 1.201 to 3.401 Å and 1.417 to 4.417 Å, respectively, with an interval step size of 0.2 Å, other geometric parameters were fully optimized. As expected, with N−O or C−N bond increasing, biradical character appears in the NCNO molecule and their dissociation PESs are contaminated by higher spin states; therefore, the unrestricted UB3LYP method was used. Meanwhile, multiconfigurational effects on the energies were also examined. Based on the structures obtained at the UB3LYP/6-311G(d) level, single point energies along the curves were performed with the third-order Rayleigh−Schrödinger perturbation theory (CASPT3)[35] and the internally contracted multireference configuration interaction method[36] using the larger 6-311+G(3df) basis set. The dissociation energies (D_0) for the NCN−O → NCN + ^{3}O and NCNO → NC + NO calculated by the CASPT3 and MRCI + Q (MRCI including Davidson's correction for higher excitations) methods are summarized in Table 2 to compare with those predicted at the G2M(CC1) level. From Table 2 one can see that the dissociation energies for NCN−O and NC−NO obtained at the G2M (CC1) level are very close to those obtained by the MRCI + Q level, the deviations are only 1.1 and 0.5 kcal/mol, respectively. However, the calculated values are around 3−4 kcal/mol higher than the experimental result, 48.9 kcal/mol.[21] On the basis of the above comparison, the dissociation curves obtained at the MRCI + Q level were used in the rate constant calculations. For the stable species and the well-defined transition states, the energies obtained at the G2M(CC1) level were used.

The dissociation curves can be fitted to the Morse potential function $E(R) = D_e\,[1 - \exp(-\beta\,(R - R_e))]$,[2] which were employed to approximate the minimum energy path for the system in our rate constant calculation. In the above equation, R is the reaction coordinate (i.e., the distance between the two bonding atoms; the N−O and C−N bonds in this work), D_e is the bond energy excluding zero-point energy, and R_e is the equilibrium value of R. The computed potential energies could be fitted reasonably to the Morse potential function with the parameter β = 2.773 Å^{-1} at the MRCI + Q(6,6)/6-311+G(3df)//UB3LYP/6-311G(d) level. For the variational curves through triplet surface, β = 3.168 Å^{-1} and 4.521 Å^{-1} for NCN + O → ^{3}NCNO and ^{3}NCON → NCO + ^{4}N processes,

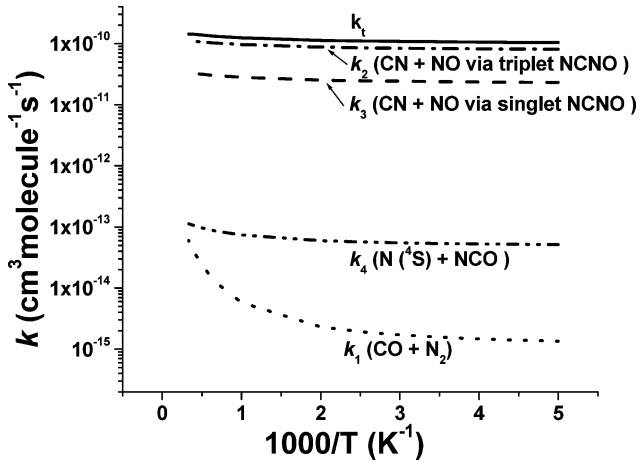

Figure 3. Predicted total and individual rate constants based on the G2M(CC1) energies. Dotted and dash−dotted lines represent the rate constants of formation CO + N_2 (k_1) and CN + NO (k_2) via singlet surface; dashed and dash−dotted−dotted lines represent the rate constants for the formation of CN + NO (k_3) and ^{4}N + NCO (k_4) via triplet surface; solid line is total rate (k_t).

respectively, which were calculated at the UB3LYP/6-311G(d) level. These values were used in all subsequent RRKM calculations.

D. Rate Constant Calculations. The component rates were evaluated with *E*, *J*-resolved RRKM calculations. For the barrierless processes, the number of a variational transition quantum states, $N^{\dagger}_{EJ}$, was given by the variationally determined minimum in $N_{EJ}(R)$, as a function of the bond length along the reaction coordinate *R*, which was evaluated according to the variable reaction coordinate flexible transition state theory.[37−40] The basis of these methods involves a separation of the vibrational modes into conserved and transitional modes. With this separation, one can evaluate the number of states by Monte Carlo integration for the convolution of the sum of vibrational quantum states for the conserved modes with the classical phase space density of states for the transitional modes.[37−40] The estimation of the transitional mode contribution to the transition state number of states for a given energy is evaluated via Monte Carlo integration with 15000 configuration numbers. The Morse potentials with the parameters mentioned in the previous section and the anisotropic potential are added together to form the final potential for the variational rate constant calculation by the Variflex code.[13] The pressure dependence was treated by 1-D master equation calculations using the Boltzmann probability of the complex for the *J* distribution. The master equation was solved by an inversion based approach.[41,42] The energy-transfer rate coefficients were computed on the basis of the exponential down model with the $\langle \Delta E \rangle$ down value of 400 cm^{-1}. To achieve convergence in the integration over the energy range, an energy grain size of 100 cm^{-1} was used, this grain size provides numerically converged results for all temperatures studies with a energy spanning range, from −32691 to 63308 cm^{-1} (relative to the reactants) for singlet channels and −26013 to 69986 cm^{-1} for triplet pathways, respectively. The total angular momentum *J* covered the range from 1 to 250 in steps of 10 for the *E*, *J*-resolved calculation. The Lennard-Jones parameters for NCNO−Ar pair were $\sigma = 3.9$ Å and $\epsilon = 205$ K, taken from ref 13. The numbers of states for the tight transition states are evaluated according to the rigid-rotor harmonic-oscillator assumption. The multiple reflection correction[43,44] above the well containing TS3, ONNC, and TS4 have been included in the rate constant calculation; a similar treatment was employed to the triplet channel, i.e., the multiple reflections above the TS13, ^{3}NCON, and the exit variational transition state producing ^{4}N + NCO (see Figure 2b).

The predicted results show that no deactivation of NCNO happened at pressures below 100 atm due to the fast exit fragmentation channel of NCNO to CN + NO. The kinetics and dynamics of the latter process have been studied in detail previously by Klippenstein.[40,45−47]

The predicted temperature-dependent rate constants are plotted in Figure 3. The results indicate that in the whole temperature range, the formation of CN + NO is dominant; its ratio is over 99% with no temperature dependence. The rate constants for the formation of CO + N_2 and ^{4}N + NCO are around 4−5 orders of magnitude lower than that for the formation of CN + NO.

The predicted individual values via the singlet surface can be presented in units of cm^3 $molecule^{-1}$ s^{-1} by

$$k_1(\mathrm{CO} + \mathrm{N_2}) = 4.03 \times 10^{-22}\, T^{2.32} \exp(571/T)$$

$$k_2(\mathrm{CN} + \mathrm{NO}) = 8.09 \times 10^{-12}\, T^{0.18} \exp(23/T)$$

and the values obtained via the triplet surface can be represented as

$$k_3(\mathrm{CN} + \mathrm{NO}) = 3.44 \times 10^{-11}\, T^{0.15} \exp(15/T)$$

$$k_4[^4\mathrm{N} + \mathrm{NCO}] = 3.67 \times 10^{-15}\, T^{0.42} \exp(79/T)$$

The total rate constant can be effectively represented by the expression

$$k_t = 4.23 \times 10^{-11}\, T^{0.15} \exp(17/T)$$

in the temperature range of 200−3000 K

Apparently, this reaction is much faster than the reaction of NCN with O_2[5] as one would anticipate.

It should be mentioned that the equilibrium constant degeneracy factors for the singlet and triplet surfaces were automatically taken into account by the code in the rate constant calculations, it can be seen from Figure 3 that the predominance of the triplet channel can be ascribed to the degeneracy of 3.

To explore the potential effects on the predicted rate, the following factors have been considered: first, because the variational entrance profiles calculated at different levels have slight differences, for example, the fitted β parameters in the Morse potential function are 2.773 and 2.686 $Å^{-1}$, respectively, at the MRCI + Q and CASPT3 levels. On the basis of $\beta = 2.773$ $Å^{-1}$, the high-pressure limit association rate constants for the O + NCN reaction on the singlet surface at 200 and 3000 K are around 6 and 5% lower than those using $\beta = 2.686$ $Å^{-1}$. Second, if the D_0 (O−NCN) is increased by 1.0 kcal/mol, the predicted rate constants vary less than 1% in the temperature range of 200−3000 K which indicates that the variational potential profiles are the crucial factor for this system. Therefore, the predicted values may be with ±10% error bar.

IV. Conclusion

The PES and mechanism for the oxidation of NCN by O have been computed at the G2M (CC1) level of theory, and the rate constants for the low-lying energy channels have been predicted. The results show that oxidation NCN by O producing CN + NO is dominant and its ratio is over 99% in the whole temperature range studied, 200−3000 K. This reaction is considerably faster than the oxidation reaction of NCN + O_2;

it is thus expected that the title reaction and OH + NCN to be studied in the near future should be the dominant oxidation processes of NCN giving rise to NO and the precursors of the prompt NO.

Acknowledgment. This work is sponsored in part by the Office of Naval Research under Contract No. N00014-02-1-0133 and in part by the Basic Energy Sciences, Department of Energy under Grant No. DE-FG-97ER14784. M.C.L. is grateful to the National Science Council of TaiWan for a Distinguished Visiting Professorship at the National Chiao Tung University, Hsinchu, Taiwan.

References and Notes

(1) Fenimore, C. P. *13th Symp (Int.) Combust. Proc*. **1971**, 373.
(2) Blauwens, J.; Smets, B.; Peeters, J. *16th Symp (Int.) Combust. Proc*. **1977**, 1055.
(3) Moskaleva, L. V.; Xia, W. S.; Lin, M. C. *Chem. Phys. Lett.* **2000**, *331*, 269.
(4) Moskaleva, L. V.; Lin, M. C. *Proc. Combust. Inst.* **2000**, *28*, 2393.
(5) Zhu, R. S.; Lin, M. C. *Int. J. Chem. Kinet.* **2005**, *37*, 593.
(6) Becke, A. D. *J. Chem. Phys.* **1993**, *98*, 5648.
(7) Becke, A. D. *J. Chem. Phys.* **1992**, *96*, 2155.
(8) Becke, A. D. *J. Chem. Phys.* **1992**, *97*, 9173.
(9) Lee, C.; Yang, W.; Parr, R. G. *Phys. Rev.* **1988**, *B37*, 785.
(10) Gonzalez, C.; Schlegel, H. B. *J. Phys. Chem.* **1989**, *90*, 2154.
(11) Mebel, A. M.; Morokuma, K.; Lin, M. C. *J. Chem. Phys.* **1995**, *103*, 7414.
(12) Frisch, M. J.; Trucks, G. W.; Head-Gordon, M.; Gill, P. M. W.; Wong, M. W.; Foresman, J. B.; Johnson, B. G.; Schlegel, H. B.; Robb, M. A.; Replogle, E. S.; Gomperts, T.; Andres, J. L.; Raghavachari, K.; Binkley, J. S.; Gonzales, C.; Martin, R. L.; Fox, D. J.; DeFrees, D. J.; Baker, J.; Stewart, J. J. P.; Pople, J. A. *Gaussian 03*, revision D.01; Gaussian, Inc.: Pittsburgh, PA, 2003.
(13) Klippenstein, S. J.; Wagner, A. F; Dunbar, R. C.; Wardlaw, D. M.; Robertson, S. H. *VARIFLEX: VERSION 1.00*, **1999**.
(14) Dorka, E. A.; Buelow, L. *J. Chem. Phys.* **1975**, *62*, 1869.
(15) Dickinson, R.; Kirby, G. W.; Sweeny, J. G.; Tyler, J. K. *J. Chem. Soc., Faraday Trans.* **1978**, *2 74*, 1393.
(16) Bak, B.; Nicolaisn, F. M.; Nielsen, O. J.; Skaarup, S. *J. Mol. Struct.* **1979**, *51*, 17.
(17) Gowenlock, B. G.; Johnson, C. A. F.; Keary, C. M.; Pfab, J. *J. Chem. Soc. Perkin Trans.* **1975**, *2 71*, 351.
(18) Pfab, J. *Chem. Phys. Lett.* **1983**, *99*, 465.
(19) Pfab, J.; Hager, J.; Krieger, W. *J. Chem. Phys.* **1983**, *78*, 266.
(20) Nadler, I.; Pfab, J.; Radhakrishnan, G.; Reisler, H.; Wittig, C. *J. Chem. Phys.* **1983**, *79*, 2088.
(21) Nadler, I; Reisler, H.; Noble, M.; Wittig, C. *Chem. Phys. Lett.* **1984**, *108*, 115.
(22) Nadler, I; Pfab, J.; Reisler, H.; Wittig, C. *J. Chem. Phys.* **1984**, *81*, 653.
(23) Noble, M.; Nadler, I; Reisler, H.; Wittig, C. *J. Chem. Phys.* **1984**, *81*, 4333.
(24) Khundkar, L. R.; Knee, J. L.; Zewail, A. H. *J. Chem. Phys.* **1987**, *87*, 77.
(25) Aray, Y.; Murgich, J.; Luna, M. A. *J. Am. Chem. Soc.* **1991**, *113*, 7135.
(26) Bai, Y. Y.; Segal, G. A. *Chem. Phys. Lett.* **1988**, *151*, 31.
(27) Dupuis, M.; Lester, W. A., Jr. *J. Chem. Phys.* **1985**, *83*, 3990.
(28) Björkman, C.; Bagus, P. S. *J. Chem. Phys.* **1982**, *76*, 3111.
(29) Jonkers, G.; Mooyman, R.; De Lange, C. A. *Chem. Phys.* **1981**, *57*, 97.
(30) Korkin, A. A.; Schleyer, P. V. R.; Boyd, R. J. *Chem. Phys. Lett.* **1994**, *227*, 312.
(31) Bise, R. T.; Choi, H.; Neumark, D. M. *J. Chem. Phys.* **1999**, *111*, 4923.
(32) Chase, M. W., Jr. *NIST-JANAF Thermochemical Tables*, 4th ed.; Woodbury, New York, 1998.
(33) Huang, Y. H.; Barts, S. A.; Halpern, J. B. *J. Phys. Chem.* **1992**, *96*, 425.
(34) Karton, A.; Rabinovich, E.; Martin, J. M. L.; Ruscic, B. *J. Chem. Phys. 2006*, 125, 144108.
(35) Werner, H. *J. Mol. Phys.* **1996**, *89*, 645.
(36) Werner, H. J.; Knowles, P. J. *J. Chem. Phys.* **1988**, *89*, 5803. Knowles, P. J.; Werner, H. J. *Chem. Phys. Lett.* **1988**, *145*, 514.
(37) Wardlaw, D. M.; Marcus, R. A. *Chem. Phys. Lett.* **1984**, *110*, 230.
(38) Wardlaw, D. M.; Marcus, R. A. *J. Chem. Phys.* **1985**, *83*, 3462.
(39) Klippenstein, S. J. *J. Phys. Chem.* **1994**, *98*, 11459.
(40) Klippenstein, S. *J. Chem. Phys. Letts.* **1990**, *170*, 71.
(41) Robertson, S. H.; Wagner, A. F.; Wardlaw, D. M. *J. Chem. Phys.* **1995**, *103*, 2917.
(42) Gilbert, R. G.; Smith, S. C. *Theory of Unimolecular Reactions*, Blackwell, 1990.
(43) Hirschfelder, J. O.; Wigner, E. *J. Chem. Phys.* **1939**, *7*, 616.
(44) Miller, W. H. *J. Chem. Phys.* **1976**, *65*, 2216.
(45) Klippenstein, S. J. *J. Chem. Phys.* **1994**, *101*, 1996.
(46) Klippenstein, S. J. *J. Chem. Phys.* **1991**, *94*, 6469.
(47) Klippenstein, S. J.; Khundkar, L. R.; Zewail, A. H.; Marcus, R. A. *J. Chem. Phys.* **1988**, *89*, 4761.